I&EC research
Industrial & Engineering Chemistry Research

Article

pubs.acs.org/IECR

Scaleup of Batch Reactors Using Phenomenological-Based Models

Gloria M. Monsalve-Bravo, Hilda M. Moscoso-Vasquez, and Hernan Alvarez*

Departamento de Procesos y Energía, Facultad de Minas, Universidad Nacional de Colombia − Sede Medellín, Medellín, Colombia

ABSTRACT: This work presents a methodology for scaling up batch processes (BPs). First, the most popular scaleup methods differentiating batch from continuous processing are reviewed, revealing that traditional scaleup approaches do not consider BP characteristics and that many particular successful cases are reported, but no formal procedure has been developed for scaling up these processes. Considering these facts, a novel scaleup procedure is presented, in which a process phenomenological-based semiphysical model (PBSM) and its Hankel matrix are used for computing the state impactability index (SII) that allow the designer to determine (i) the main process dynamics at each stage of the batch and (ii) the critical point of the operating trajectory (OT) at which the batch must be scaled up. Finally, the methodology is applied to a batch suspension polymerization reactor, comparing the scaled unit design using this approximation and a traditional method.

1. INTRODUCTION

Batch processes (BPs) are considered to be important in the chemical industry, especially when low production volumes or a great variety of products within a single process unit are required.[1−3] Although this kind of processing represents the natural way to increase process capacity from the laboratory to a commercial unit,[4,5] continuous processes (CPs) have dominated research works in the scaleup field.[2,6−8]

Neither particular nor generalizable progress has been reported in the field of the scaleup of chemical processes. Such processes are still scaled up using traditional methods that have not changed significantly since the 1960s.[9−14] Industrial scaleup is dominated by empirical scaleup rules, requiring geometrical similarity with criteria such as equal tip speed or equal mass-transfer coefficients, leading to drawbacks from keeping a single parameter constant.[5,12,15,16] Here, given that some parameters are fixed, the rest could change substantially in unforeseen ways,[8,17] resulting in an erroneous commercial unit design requiring additional costs and time to be corrected.[9,18]

Although there is no particular literature on the scaleup of BPs, the same methods are used for both batch and continuous processes.[10,12,13,19,20] For batch processing, a combination of scaleup methods such as similarity criteria, dimensional analysis, and general guidelines is usually employed to obtain an acceptable unit design at a new operating scale.[6,17,18] In practice, no single design protocol can be universally applied to all process units.[14,21] Therefore, no general rule exists for scaling up chemical processes and a huge effort and great level of skill are required to achieve the same conversion, selectivity, and product distribution at an industrial scale as reached at the laboratory scale.[8,12,15]

Although the use of phenomenological-based models in the scaleup field has increased in the past few years,[15,19,22,23] it is significantly inconvenient when validating a model at several operating scales, especially because model parameters such as transfer coefficients (mass, heat, and momentum) vary when scale changes.[8,9,24−26] In addition, when the studied system is considered to be complex, the designer is forced to use optimization algorithms to find optimal parameters, which results in an impractical, arduous, and boundless task.[15,18,20,27] This also evidences the lack of a procedure that facilitates the task of finding these parameters.

Therefore, considering that fundamental models that are able to describe key characteristics of the process are perhaps the most helpful tool for establishing optimal process conditions and scaling it up,[9,15,19,28] this work presents a novel methodology for scaling up BPs using (i) a phenomenological-based semiphysical model (PBSM) for representing the process, and (ii) the process Hankel matrix (widely used in model reduction,[29] system identification, digital filter design, model order determination,[30] and controller design[31]) as a tool for establishing a dynamics hierarchy and real scale factors, by means of the state impactability index (SII). This index provides a quantitative measure of the significance of each state variable in the process (a dynamics hierarchy) and, hence, the most impacted state variable by the scale increments. By means of its calculation, it is possible to establish the critical point of the operating trajectory (OT) at which the batch must be scaled up.

The article is organized as follows: First, scaleup methods are briefly reviewed considering the differences between batch and continuous processes, analyzing their limitations concerning BPs. Then, the methodology for scaling up BPs is presented using both a process PBSM and its Hankel matrix. Finally, the proposed methodology is applied to a methyl methacrylate (MMA) batch suspension polymerization reactor, establishing the scaled unit design with the same OT set at the current scale and the dynamics hierarchy at both scales.

2. SCALEUP OF BATCH PROCESSES

It is possible to distinguish three basic approaches in the scaleup procedure.[9,12,24,32,33] The first is known as the physical approach. This approach involves the use of dimensionless numbers, variables, and relationships to relate the same process

Received: February 10, 2014
Revised: April 15, 2014
Accepted: April 24, 2014

   dx.doi.org/10.1021/ie500587r | *Ind. Eng. Chem. Res.* XXXX, XXX, XXX−XXX

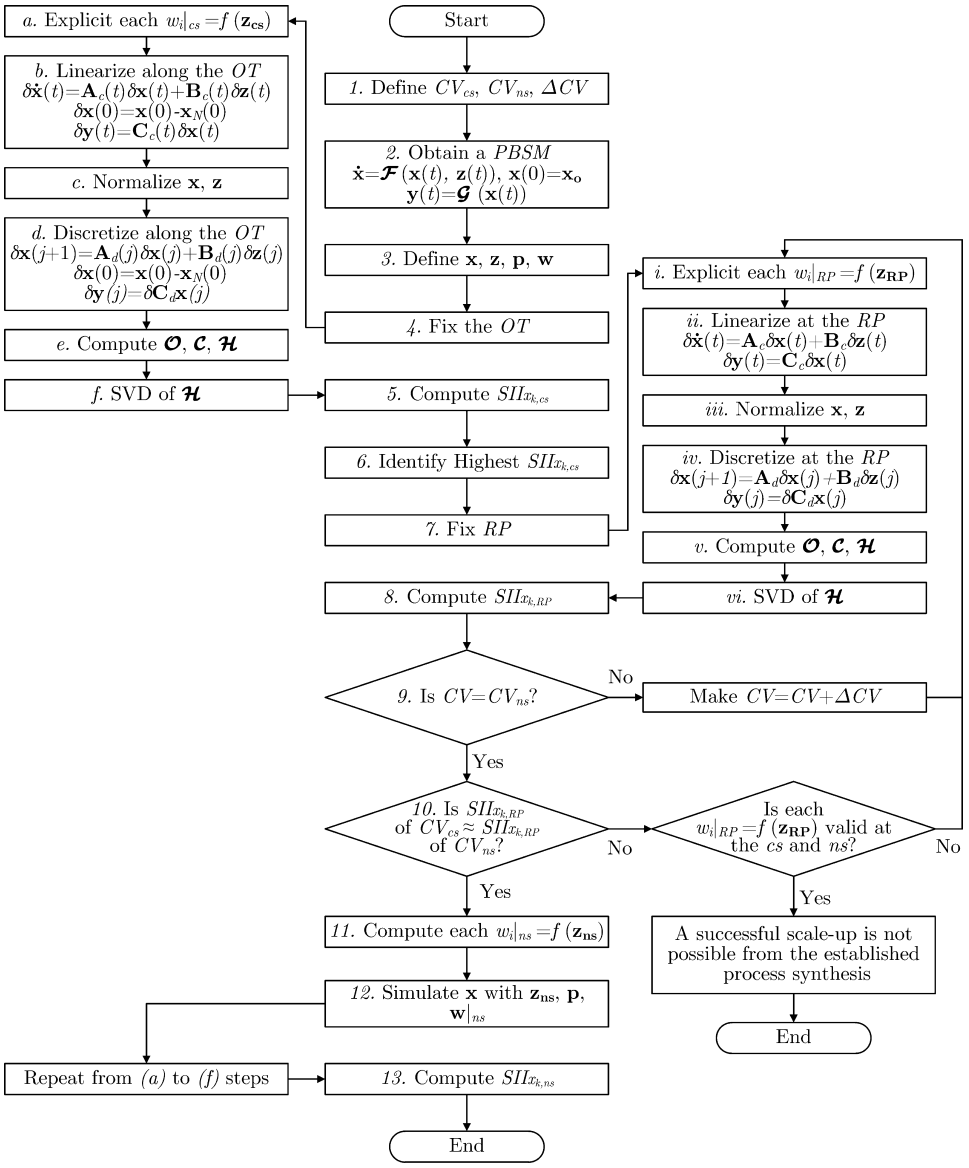

Figure 1. Proposed procedure for scaleup.

at different scales.[7,10,34] These dimensionless numbers or groups of variables form the basis for scaling up from one size to another.[11,23,35] Two different methods can be followed in the context of the physical approach:[16,32] (i) similarity criteria, which include (a) geometrical, (b) mechanical, (c) thermal, and (d) chemical similarities,[23,34] and (ii) dimensional analysis, which includes (a) Buckingham π-theorem based method and (b) inspectional analysis that uses a dimensionless form of the governing equations.[7,11,35]

The second is the experimental approach, in which designer knowledge about a particular process is used for carrying out its scaleup.[9,24,32,33] This approach involves sequential scaleup studies, each increment building on the knowledge gained in the previous one.[14,36,37] The experimental approach offers a low scaleup ratio, which results in a large number of experiments, which is highly expensive if a large scale must be achieved.[24] Two different methods can be followed in the context of the experimental approach: (i) trial and error, in which experimental process data are used for the construction of empirical relations,[32,37] and (ii) rules of thumb that consider a constant value of a particular operating parameter as a general rule during the scaleup.[6,13−15]

The third is called the fundamental approach. This approach involves proper modeling of the process under consideration.[9,15,25,33] It is based on the use of a PBSM for the description of the process dynamics,[19,26,32] generating an excellent process understanding and allowing for a process to be scaled up by more than 1000 times, quickly and reliably.[9,24] Two different methods can be followed in the context of this approach: (i) simulations with variation of parameters[6,15,22,32] and (ii) the use of a dynamics hierarchy (Hankel matrix).[9,33] The extension of the latter to the scaleup of BPs is the focus of this work.

Although BPs represent an antique, flexible, and versatile operating mode,[2,3] widely used to obtain high-value products,[1] they are still scaled up using traditional methods (experimental and physical approaches),[12,17,18] leading to unforeseen problems (adjustment of equipment and operating conditions) and additional production costs.[38] Three major differences between batch and continuous processes must be considered to scale up a batch unit.

dx.doi.org/10.1021/ie500587r | Ind. Eng. Chem. Res. XXXX, XXX, XXX−XXX

The first difference is related to the operating point. CPs have a single operating point, which means that they have time-constant characteristics. In contrast, BPs have a dynamic operating point, which means that they have time-varying characteristics.[4,17] Given that BPs involve chemical transformations that proceed from an initial state to a highly different final state,[39] there is no unique operating point around which the process can be scaled up as is the case for CPs.[40] In this way, as a consequence of the time-varying characteristics of BPs, kinetic reaction and transfer coefficients change significantly during a batch, forcing the designer to determine by expertise which mechanism is governing each stage of the batch to scale up the process.[5,17]

The second difference is related to the nonlinear behavior. Both BPs and CPs can exhibit this behavior for a variety of reasons, the two major ones of which are (i) the nonlinear relation between the reaction rates with concentrations (often) and with temperature (always) and (ii) the nonlinear relationship between the transport-phenomena-dependent parameters and the inside-reactor properties.[4] However, in CPs, there is a unique rate-limiting stage because they have a single operating point, so their inside-reactor properties remain constant during the process time.[17] Instead, in BPs, the inside-reactor properties change significantly during the batch time, causing changes in the transfer coefficients and, hence, the existence of various rate-limiting stages. The dominance of these stages must be established to scale up this type of process. Here, a given phenomenon that governs the process dynamics during a finite period of time is considered as a rate-limiting stage.

Finally, the third difference is related to the presence of constraints. Although all manipulated variables in both BPs and CPs are physically constrained, BPs also exhibit operating constraints[1,2,40] that must be considered when scaling up the process. Here, the dynamic nature of BPs is the source of internal disturbances and, hence, the need to be constrained for safety, quality, or stability reasons.[39] For instance, in exothermic batch polymerization reactors, a common industrial practice is to maintain isothermal operation (at low temperature) for the batch safety. Although higher temperatures can reduce the reaction time by increasing the polymerization reaction rates, a temperature increase results in an excess of heat that raises the risk of a thermal runaway and also produces polymer of lower molecular weight.[41] Therefore, there must be an equilibrium point between productivity on one hand and safety, stability, and quality on the other, for the selection of the reactor temperature.[40] Furthermore, because of the wide operating range of BPs, it is rarely possible to design and operate this type of process away from constraints, as is typically done for CPs.[4]

3. PROPOSED PROCEDURE FOR SCALEUP

As a way to overcome the limitations mentioned in the previous section during the scaleup of BPs and considering that a PBSM is the most useful tool for scaling up chemical processes,[9,15,26] Figure 1 presents the proposed methodology for scaling up BPs. The 13 steps of the procedure are described as follows.

Step 1: The capacity variables at the current scale (CV_{cs}) and the new scale (CV_{ns}) and the capacity variable step (ΔCV) are defined. A definition of CV is given as follows.

Definition 1. A capacity variable (CV) is any process variable indicating a processing capacity of a process unit. It is associated with process holdup or an extensive variable.

Step 2: A PBSM of the process is obtained, using the methodology developed by Alvarez et al.[28] The obtained model has the following layout

$$\dot{\mathbf{x}} = \mathcal{F}(\mathbf{x}(t), \mathbf{z}(t)), \quad \mathbf{x}(0) = \mathbf{x}_0 \tag{1}$$

$$\mathbf{y}(t) = \mathcal{G}(\mathbf{x}(t)) \tag{2}$$

where $\mathbf{x}(t) \in \mathcal{R}^n$ is the system state space vector, $\mathbf{z}(t) \in \mathcal{R}^p$ is the design variable space vector, $\mathbf{y}(t) \in \mathcal{R}^m$ is the system output space vector, and $\mathbf{x}_0$ is the initial state vector. Considering that a model is a simplified representation of the real process, the model needs to be validated at the current scale (cs) to represent the process at the new scale (ns). Therefore, by using a validated PBSM at the cs, the dynamic behavior of the process at the cs is transferred to the ns by means of the proposed procedure. Here, the PBSM structure (material and energy balances) enables the model to be valid at both scales.

Step 3: State variables ($\mathbf{x}$), design variables ($\mathbf{z}$), synthesis parameters ($\mathbf{p}$), and design-variable-dependent parameters ($\mathbf{w}$) are defined from the obtained model. Definitions of $\mathbf{x}$, $\mathbf{z}$, $\mathbf{p}$, and $\mathbf{w}$ are given next.

Definition 2. State variables ($\mathbf{x}$) are the smallest set of variables that must be specified at time $t = t_0$ to predict the behavior of the process for any time $t \geq t_0$.[42]

Definition 3. Design variables ($\mathbf{z}$) are the variables whose values can be freely varied by the designer to define a designed process.

Definition 4. Synthesis parameters ($\mathbf{p}$) are characteristic (inherent) parameters of the process, set from the process conception. Once established, they remain fixed during the scaleup.

Definition 5. Design-variable-dependent parameters ($\mathbf{w}$) are the parameters that depend on the design variables ($\mathbf{z}$); that is, $\mathbf{w}$ can be written as an explicit function of $\mathbf{z}$.

Step 4: The operating trajectory (OT) is fixed. A definition of OT is given as follows.

Definition 6. The operating trajectory (OT) is the value of the state vector at each time instant. The OT is obtained by solving the mathematical model including the adequate values of the manipulated input variables.

It is assumed that the nominal OT is known from process synthesis at the cs and the proposed methodology does not optimize it. Thus, this trajectory must be properly chosen to carry out the scaleup. The works of Bonvin and co-workers[4,40] describe the main issues for determining the optimal OT of a batch process.

Intermediate steps: These steps are followed to compute the state impactability index of each state variable at the current scale ($SII_{x_{i,cs}}$).

(a) An equation for each $w_i|_{cs} = f(\mathbf{z}_{cs})$ is found. These expressions only need to be valid at the cs to represent the process dynamic behavior at this scale.

(b) It is assumed that the process dynamics, in the immediate proximity of the nominal OT, can be approximated by the first terms of the Taylor series. Thus, the model is linearized along the OT, discretizing it on a number of finite points so a continuous linear model ensemble can represent the OT, as shown in the equations

$$\delta\dot{\mathbf{x}}(t) = \mathbf{A}_c(t)\,\delta\mathbf{x}(t) + \mathbf{B}_c(t)\,\delta\mathbf{z}(t), \quad \delta\mathbf{x}(0) = \mathbf{x}(0) - \mathbf{x}_N(0) \tag{3}$$

dx.doi.org/10.1021/ie500587r | Ind. Eng. Chem. Res. XXXX, XXX, XXX−XXX

$$\delta\mathbf{y}(t) = \mathbf{C}_c(t)\,\delta\mathbf{x}(t) \tag{4}$$

where $\mathbf{A}_c = \partial\mathcal{F}/\partial\mathbf{x}|_{\mathbf{x}_N,\mathbf{z}_N}$, $\mathbf{B}_c = \partial\mathcal{F}/\partial\mathbf{z}|_{\mathbf{x}_N,\mathbf{z}_N}$, and $\mathbf{C}_c = \partial\mathcal{G}/\partial\mathbf{x}|_{\mathbf{x}_N,\mathbf{z}_N}$ are the Jacobian matrices of the continuous linear systems. The subscript N represents the nominal OT.

(c) $\mathbf{B}_c$ and $\mathbf{C}_c$ are modified to make both design and output variables dimensionless and normalized, as follows

$$\bar{b}_{ij} = b_{ij}(z_{j,\max} - z_{j,\min}) \tag{5}$$

$$\bar{c}_{ij} = \frac{c_{ij}}{(y_{i,\max} - y_{i,\min})} \tag{6}$$

Here, $\mathbf{A}_c$ is not altered because the Hankel matrix is a tool that considers only the inputs and outputs of the system,[43] so any mathematical operation on $\mathbf{x}$ will be annulled during the Hankel matrix calculation.[31]

The subscripts max and min indicate the maximum and minimum values of z_j and y_i in each case. They are established from the process synthesis based on the knowledge of the process design and desired performance targets. If these limits are not adequately chosen, the dynamics hierarchy could be altered, and hence, the selection of the main dynamics might be wrong. Here, $z_{j,\min}$ and $z_{j,\max}$ might depend on the scale, whereas $y_{i,\min}$ and $y_{i,\max}$ do not. Also, the system is considered to be completely observable, or its state is considered to be fully measured, which leads to $\mathbf{C}_c$ being the identity matrix and y_i and x_i having the same limits.

(d) Linear models at each point of the OT are discretized. Here, the sampling time (t_s) must be chosen carefully so that each discrete model is able to represent each continuous one. The layout of the ensemble of models is presented as follows

$$\delta\mathbf{x}(j+1) = \mathbf{A}_d(j)\,\delta\mathbf{x}(j) + \mathbf{B}_d(j)\,\delta\mathbf{z}(j),\quad \delta\mathbf{x}(0) = \mathbf{x}(0) - \mathbf{x}_N(0) \tag{7}$$

$$\delta\mathbf{y}(j) = \mathbf{C}_d(j)\,\delta\mathbf{x}(j) \tag{8}$$

where $\mathbf{A}_d = \mathbf{I} + \mathbf{A}_c t_s$, $\mathbf{B}_d = t_s\mathbf{B}_c$, and $\mathbf{C}_d = \mathbf{C}_c$ are process discrete matrices.

(e) The observability ($\boldsymbol{O} \in \mathcal{R}^{nm\times n}$), controllability ($\boldsymbol{C} \in \mathcal{R}^{n\times np}$), and Hankel ($\mathcal{H} \in \mathcal{R}^{nm\times np}$) matrices are computed for each discrete model as follows

$$\boldsymbol{O}(j) = [\mathbf{C}_d(j)\ \ \mathbf{C}_d(j)\mathbf{A}_d(j)\ \ \mathbf{C}_d(j)\mathbf{A}_d{}^2(j)\ \ \cdots\ \ \mathbf{C}_d(j)\mathbf{A}_d{}^{n-1}(j)]^T \tag{9}$$

$$\boldsymbol{C}(j) = [\mathbf{B}_d(j)\ \ \mathbf{A}_d(j)\mathbf{B}_d(j)\ \ \mathbf{A}_d{}^2(j)\mathbf{B}_d(j)\ \ \cdots\ \ \mathbf{A}_d{}^{n-1}\mathbf{B}_d(j)] \tag{10}$$

$$\mathcal{H}(j) = \boldsymbol{O}(j)\,\boldsymbol{C}(j) \tag{11}$$

(f) $\mathcal{H}$ is decomposed into singular values according to

$$\mathcal{H}(j) = \mathbf{U}(j)\,\boldsymbol{\Sigma}(j)\,\mathbf{V}^T(j) \tag{12}$$

where the matrices $\mathbf{U} \in \mathcal{R}^{nm\times nm}$ and $\mathbf{V} \in \mathcal{R}^{np\times np}$ are the column and row spaces, respectively, of $\mathcal{H}$. Also, the diagonal elements of $\boldsymbol{\Sigma} \in \mathcal{R}^{nm\times np}$ are the singular values (σ_{ii}) of $\mathcal{H}$.

Step 5: The state impactability index of each state variable (SII_{x_k}), which represents the impactability of the process design variables ($\mathbf{z}$) as a whole over a kth given state variable (x_k), is computed as

$$\mathrm{SII}_{x_k}(j) = \sqrt{\sum_{i=1}^{r}\sigma_{ii}{}^2(j)\Big[\sum_{s=0}^{n-1}U_{k+ns,i}{}^2(j)\Big]},\quad k = 1, 2, \ldots, n \tag{13}$$

where r is the rank of $\mathcal{H}$ (i.e., the number of nonzero σ_{ii} values). In this way, the main dynamics (the most impacted dynamics) is the x_k with the highest SII along the batch. The SII_{x_k} values also determine the operating regime (OR) along the batch, which corresponds to the dynamics hierarchy obtained at each point where the process is linearized, according to definition 7.

Definition 7. The operating regime (OR) is a quantitative hierarchical relation among the state variables of the process at a given point of the operating trajectory (OT). This relation is established by the calculation of the state impactability index (SII) of each state variable, which includes the effect of the design variables as a whole on each state variable at each point of the OT.

Step 6: The critical point of the batch is identified. It corresponds to the highest point of the SII profile for the main dynamics.

Step 7: The batch critical point is selected as the reference point (RP) for scaling up the process. Therefore, for any point with an SII value less than SII_{RP}, the process requirements are fulfilled, considering that the requirements were fulfilled at the RP.

Intermediate Steps i–vi: These steps are followed, using eqs 3–12, to determine the state impactability index of each state variable at the reference point ($\mathrm{SII}_{x_{k,RP}}$) as the scale is increased. Here, in intermediate step i, each $w_i|_{RP} = f(\mathbf{z_{RP}})$ must be valid at all scales from the cs to the ns for the model to be able to represent the process at both scales in the RP.

Step 8: $\mathrm{SII}_{x_{k,RP}}$ is computed using eq 13.

Step 9: Steps i–vi and 8 are repeated until CV = CV_{ns}. Here, the components of $\mathbf{w}|_{RP}$ are computed with scale increments, allowing for the process to be scaled up at the RP.

Step 10: Each $\mathrm{SII}_{x_{k,RP}}$ value is compared at the cs and ns. If the values are equal at both scales, continue with step 11. Otherwise, that is, if at least one of $\mathrm{SII}_{x_{k,RP}}$ values is outside the interval $[0.9\mathrm{SII}_{x_{k,RP}},\ 1.1\mathrm{SII}_{x_{k,RP}}]$ at the ns ($\mathbf{x}$ and hence SII are expected to have small changes), each $w_i|_{RP} = f(\mathbf{z_{RP}})$ must be reviewed (see Figure 1). If these equations are valid at both scales, a successful scaleup is not possible from the established process synthesis. Therefore, the process synthesis must be reviewed. Otherwise, change the corresponding nonvalid equations and recompute steps i–vi, 8, and 9. Here, given that the SII is a quantitative measure of the batch behavior, it allows the designer to determine the effect on the quality targets of designing a specific unit (obtained, for instance, by traditional methods) instead of the required one by the process dynamics. Also, if the SII is altered by scale increments, the process behavior degrades. Therefore, the wider the $\mathrm{SII}_{x_{k,RP}}$ interval, the greater the risk of not reproducing the dynamic behavior of the process at the ns.

Step 11: Given that values for each $w_i|_{RP}$ are determined at the ns, to obtain the exact scaled unit design that matches each $w_i|_{RP}$ requirement, an equation for each $w_i|_{ns} = f(\mathbf{z}_{ns})$ is established. Here, these expressions need to be valid only at the ns.

dx.doi.org/10.1021/ie500587r | Ind. Eng. Chem. Res. XXXX, XXX, XXX–XXX

Step 12: The process is simulated with $\mathbf{p}$, $\mathbf{z}_{ns}$, and $\mathbf{w}|_{ns}$ to verify that the process at the ns achieved the same performance targets as were set at the cs.

Intermediate Steps a−f: These steps are followed, using eqs 3−12, to compute the state impactability index of each state variable at the new scale ($SII_{x_{k,ns}}$).

Step 13: $SII_{x_{k,ns}}$ is computed using eq 13. During this step, one can establish whether the designed unit is over- or undersized by comparing the $SII_{x_{k,cs}}$ and $SII_{x_{k,ns}}$ profiles. The last two steps are performed to verify that the process at the ns reproduces the dynamic behavior of the cs.

4. SCALEUP OF A BATCH POLYMERIZATION REACTOR

The literature shows that there is no simple rule or procedure for scaling up suspension polymerization reactors;[44,45] rather, combinations of the methods described in section 2 have been used when scaling up this type of process.[46,47] Therefore, in this section, a batch suspension polymerization reactor is scaled up, comparing the proposed methodology with a traditional method. Even though a PBSM must be validated at the cs to use the methodology, in this section, a complete PBSM is used as a real process and a simplified one for scaling up the process. Thus, the scaleup task is verified by means of the complete model.

4.1. Modeling of the Batch Suspension Polymerization Reactor.

The model proposed herein was obtained using the methodology of Alvarez et al.[28] Figure 2 shows the process flow diagram. Because polymerization reactions are highly exothermic, the reactor is cooled using a double-pipe heat exchanger in series with the reactor jacket that maintains its temperature at 358.15 K.

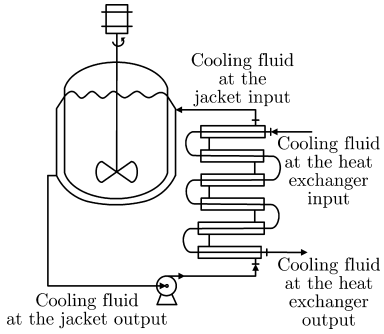

Figure 2. Flow diagram of the batch polymerization reactor process.

During the polymerization, it is assumed that the following kinetic mechanism governs the PMMA synthesis[45,47,48]

$$\mathrm{I} \xrightarrow{k_d} 2\mathrm{R} \tag{14}$$

$$\mathrm{M} + \mathrm{R} \xrightarrow{k_i} \mathrm{P}_1 \tag{15}$$

$$\mathrm{P}_\alpha + \mathrm{M} \xrightarrow{k_{pg}} \mathrm{P}_{\alpha+1} \tag{16}$$

$$\mathrm{P}_\alpha + \mathrm{M} \xrightarrow{k_{fm}} \mathrm{P}_1 + \mathrm{D}_\alpha \tag{17}$$

$$\mathrm{P}_\alpha + \mathrm{P}_\beta \xrightarrow{k_{tc}} \mathrm{D}_{\alpha+\beta} \tag{18}$$

$$\mathrm{P}_\alpha + \mathrm{P}_\beta \xrightarrow{k_{td}} \mathrm{D}_\alpha + \mathrm{D}_\beta \tag{19}$$

Here, I, R, and M represent the initiator, primary radical, and monomer species, respectively. P_α, P_β and D_α, D_β are the live and dead polymer chains, respectively, where α and β represent chains with different lengths. k_d, k_i, k_{pg}, k_{fm}, k_{tc}, and k_{td} are the kinetic constants for decomposition, initiation, propagation, chain transfer to polymer, termination by recombination, and termination by disproportionation, respectively.

Based on the free-radical mechanism shown in eqs 14−19, a model composed of an infinite number of radical population equations is obtained. Therefore, to simplify the infinite number of radical population equations (P_1, P_2, ..., P_α, P_β and D_1, D_2, ..., D_α, D_β) into a smaller set of modeling equations,[45,49,50] eq 20 is used to compute the zeroth (λ_0), first (λ_1), and second (λ_2) moments of the live polymer chains, and eq 21 is used to compute the zeroth (η_0), first (η_1), and second (η_2) moments of the dead polymer chains

$$\lambda_\gamma = \sum_{\alpha=1}^{\infty} \alpha^\gamma P_\alpha \tag{20}$$

$$\eta_\gamma = \sum_{\alpha=1}^{\infty} \alpha^\gamma D_\alpha \tag{21}$$

where $\gamma = 0, 1, 2$, and P_α and D_α represent the concentrations of the corresponding species. According to this approach, a reduced model composed of differential eqs 22−34 and algebraic eqs 35−121 is obtained. Units of measurement for all of the variables and parameters are given in the Nomenclature section.

$$\frac{dI}{dt} = -k_d I \tag{22}$$

$$\frac{dR}{dt} = 2fk_d I - k_i MR \tag{23}$$

$$\frac{dM}{dt} = -k_i MR - (k_{pg} + k_{fm})M\lambda_0 \tag{24}$$

$$\frac{d\lambda_0}{dt} = k_i MR - (k_{tc} + k_{td})\lambda_0^2 \tag{25}$$

$$\frac{d\lambda_1}{dt} = k_i MR + k_{pg}M\lambda_0 + k_{fm}M(\lambda_0 - \lambda_1) - (k_{tc} + k_{td})\lambda_0 \lambda_1 \tag{26}$$

$$\frac{d\lambda_2}{dt} = k_i MR + k_{pg}M(\lambda_0 + 2\lambda_1) + k_{fm}M(\lambda_0 - \lambda_2) - (k_{tc} + k_{td})\lambda_0\lambda_2 \tag{27}$$

$$\frac{d\eta_0}{dt} = k_{fm}M\lambda_0 + \left(k_{td} + \frac{1}{2}k_{tc}\right)\lambda_0^2 \tag{28}$$

$$\frac{d\eta_1}{dt} = k_{fm}M\lambda_1 + (k_{td} + k_{tc})\lambda_0\lambda_1 \tag{29}$$

$$\frac{d\eta_2}{dt} = k_{fm}M\lambda_2 + k_{td}\lambda_0\lambda_2 + k_{tc}(\lambda_0\lambda_2 + \lambda_1^2) \tag{30}$$

$$\frac{dT_r}{dt} = \frac{1}{C_{p,r}\rho_r V_r}[-k_{pg}M\lambda_0(-\Delta H_p)V_r - \dot{Q}_1] \tag{31}$$

dx.doi.org/10.1021/ie500587r | Ind. Eng. Chem. Res. XXXX, XXX, XXX−XXX

$$\frac{dT_2}{dt} = \frac{1}{C_{p,2}\rho_2 V_j}[F_1\rho_1 C_{p,1}(T_1 - T_{ref}) - F_2\rho_2 C_{p,2}(T_2 - T_{ref}) + \dot{Q}_1] \quad (32)$$

$$\frac{dT_1}{dt} = \frac{1}{C_{p,1}\rho_1 V_a}[F_2\rho_2 C_{p,2}(T_2 - T_{ref}) - F_1\rho_1 C_{p,1}(T_1 - T_{ref}) - \dot{Q}_2] \quad (33)$$

$$\frac{dT_4}{dt} = \frac{1}{C_{p,4}\rho_4 V_t}[F_3\rho_3 C_{p,3}(T_3 - T_{ref}) - F_4\rho_4 C_{p,4}(T_4 - T_{ref}) + \dot{Q}_2] \quad (34)$$

where T_r is the reactor temperature; T_1 and T_2 are the cooling fluid temperatures at the jacket input and output, respectively; and T_4 is the cooling fluid temperature at the inner tube output of the heat exchanger.

In eqs 22−31, f represents the initiator efficiency, and ΔH_p is the heat of polymerization. Also, kinetic constants, k_d, k_I, k_{pg}, k_{fm}, k_p, k_{tc}, and k_{td}, are obtained as follows[49,51]

$$k_d = 1.014 \times 10^{16} e^{-30000/R_g T_r} \quad (35)$$

$$k_I = k_{pg} = 2.95 \times 10^7 e^{-4350/R_g T_r} \quad (36)$$

$$k_{fm} = 9.48 \times 10^3 k_{pg} e^{-13880/R_g T_r} \quad (37)$$

$$k_t = 5.88 \times 10^9 e^{-701/R_g T_r} \quad (38)$$

$$k_{td} = k_t - k_{tc} \quad (39)$$

$$k_{tc} = 3.956 \times 10^{-4} k_{td} e^{4090/R_g T_r} \quad (40)$$

Here, k_t is the termination constant rate, and R_g is the ideal gas constant. The reactor fluid (ρ_r) density is given by[52,53]

$$\rho_r = \frac{\rho_{r,0}}{1 + \epsilon X_m} \quad (41)$$

where $\rho_{r,0}$ is the initial density of the reactor fluid and X_m represents the monomer conversion, given by[52,54]

$$X_m = \frac{M_0 - M}{M_0 + \epsilon M} \quad (42)$$

where M_0 is the initial monomer concentration. Also, the contraction factor (ϵ) can be computed as[54,55]

$$\epsilon = \left(\frac{\rho_m}{\rho_p} - 1\right)\phi_{m,0} \quad (43)$$

where $\phi_{m,0}$ is the initial volume fraction of monomer. The densities of the monomer (ρ_m) and polymer (ρ_p) can be calculated using the equations[56,57]

$$\rho_m = 968 - 1.225(T_r - 273.15) \quad (44)$$

$$\rho_p = 1212 - 0.845(T_r - 273.15) \quad (45)$$

In eqs 32−34, the densities of the cooling fluid at the jacket input (ρ_1) and output (ρ_2) are obtained from eqs 46 and 47,[58] respectively, and those at the inner tube input (ρ_3) and output (ρ_4) are computed using eqs 48 and 49, respectively.[56]

$$\rho_1 = 1309.6 - 0.73677T_1 \quad (46)$$

$$\rho_2 = 1309.6 - 0.73677T_2 \quad (47)$$

$$\rho_3 = 1011 - 0.4484(T_3 - 273.15) \quad (48)$$

$$\rho_4 = 1011 - 0.4484(T_4 - 273.15) \quad (49)$$

In addition, the cooling fluid flow rate at the jacket output (F_2) is given by eq 50, and the cooling fluid flow rates at the inner tube input (F_3) and output (F_4) are given by eqs 52 and 51, respectively

$$F_2 = F_1\frac{\rho_1}{\rho_2} \quad (50)$$

$$F_4 = F_3\frac{\rho_3}{\rho_4} \quad (51)$$

$$F_3 = F_{3,bias} + K_{pe}(t) + K_I\int_{t_0}^{t} e(t)\,dt + K_D\frac{de(t)}{dt} \quad (52)$$

where F_1 is the cooling fluid flow rate at the jacket input and $F_{3,bias}$ is the nominal cooling fluid flow rate at the inner tube. K_P, K_I, and K_D are the proportional, integral, and derivative controller gains, respectively, and $e(t) = T_{r,sp} - T_r$, where the subscript sp represents the set point. On the other hand, in eq 31, the reactor fluid specific heat capacity ($C_{p,r}$) is given by

$$C_{p,r} = \phi_m C_{p,m} + \phi_p C_{p,p} + \phi_s C_{p,s} \quad (53)$$

considering that the use of volume fractions for computing mixture properties is a common practice when modeling polymerization processes.[49,53] Here, $C_{p,m}$, $C_{p,p}$ and $C_{p,s}$ are the specific heat capacities of the monomer, polymer, and water, respectively, and the volume fractions of monomer (ϕ_m), polymer (ϕ_p), and water (ϕ_s) are given by[50]

$$\phi_m = \left(\frac{1 - X_m}{1 + \epsilon X_m}\right)\phi_{m,0} \quad (54)$$

$$\phi_p = \phi_{m,0} - \phi_m \quad (55)$$

$$\phi_s = 1 - \phi_p - \phi_m \quad (56)$$

The specific heat capacities of the cooling fluid at the jacket input ($C_{p,1}$) and output ($C_{p,2}$) are given by[58]

$$C_{p,1} = 1.64 \times 10^3 + 7.06T_1 - 5.71 \times 10^{-3}T_1^2 \quad (57)$$

$$C_{p,2} = 1.64 \times 10^3 + 7.06T_2 - 5.71 \times 10^{-3}T_2^2 \quad (58)$$

and those at the inner tube input ($C_{p,3}$) and output ($C_{p,4}$) are given by[59]

$$C_{p,3} = 1.02 \times 10^3 + 2.63 \times 10^1 T_3 - 7.45 \times 10^{-2}T_3^2 + 7.28 \times 10^{-5}T_3^3 \quad (59)$$

$$C_{p,4} = 1.02 \times 10^3 + 2.63 \times 10^1 T_4 - 7.45 \times 10^{-2}T_4^2 + 7.28 \times 10^{-5}T_4^3 \quad (60)$$

The heat-transfer rates at the reactor ($\dot{Q}_1$) and at the double-pipe heat exchanger ($\dot{Q}_2$) can be calculated using the equations[60,61]

dx.doi.org/10.1021/ie500587r | Ind. Eng. Chem. Res. XXXX, XXX, XXX−XXX

$$\dot{Q}_1 = U_r A_r (T_r - T_2) \tag{61}$$

$$\dot{Q}_2 = U_{he} A_t N_{hp} (T_1 - T_4) \tag{62}$$

where N_{hp} is the number of hairpins. Also, the overall heat-transfer coefficients at the reactor (U_r) and heat exchanger (U_{he}) are given by[60,61]

$$U_r = \frac{1}{\frac{1}{h_r} + \frac{T}{2k_{w,r}} \ln\left(\frac{D_{ji}}{T}\right) + \frac{1}{h_j}\frac{T}{D_{ji}}} \tag{63}$$

$$U_{he} = \frac{1}{\frac{1}{h_t}\frac{A_t}{A_i} + \frac{A_t}{A_i} R_{fi} + \frac{A_t}{2\pi d_i k_{w,he} 2L_t} \ln\left(\frac{d_o}{d_i}\right) + \frac{R_{fo}}{\xi_o} + \frac{1}{\xi_o h_a}} \tag{64}$$

Note that eqs 63 and 64 are valid only for the current-scale design. Therefore, in the following subsection, eq 63 is replaced by an expression that is valid at all scales, and 64 is changed according to the requirements of the new scale. $k_{w,r}$ and $k_{w,he}$ are the thermal conductivities of the reactor wall and heat-exchanger pipe, respectively. T is the tank diameter, and D_{ij} is the inner diameter of the annular jacket. d_i and d_o are inside and outside diameters, respectively, of the heat-exchanger inner tube, and L_t is the nominal length of the exchange section. R_{fi} and R_{fo} are the fouling resistances of the inner tube and annulus, respectively. Also, in eq 61, A_r is the reactor transfer area, given by

$$A_r = \pi T Z + \frac{\pi}{4} T^2 \tag{65}$$

Here, the reactor fluid height (Z) can be computed as

$$Z = \frac{4(V_r - V_{bottom})}{\pi T^2} \tag{66}$$

where the reactor volume (V_r) is given by[50]

$$V_r = V_{r,0}(1 + \epsilon X_m) \tag{67}$$

Also, $V_{r,0}$ is the initial reactor volume, and V_{bottom} the volume of the reactor bottom. In addition, in eq 32, V_j is the jacket volume, calculated as

$$V_j = \frac{2}{5} V_r \tag{68}$$

In 64, A_t is the overall outside area of the inner tube, given by

$$A_t = A_u + A_f \tag{69}$$

where the outside area of the inner tube (A_u) and the area of a fin (A_f) are calculated as

$$A_u = 2(\pi d_o L_t - N_f L_t \delta_f) \tag{70}$$

$$A_f = 2N_f L_t (2H_f + \delta_f) \tag{71}$$

Also, A_i is the inside area of the inner tube, computed as[60]

$$A_i = 2\pi d_i L_t \tag{72}$$

where N_f is the number of fins and δ_f is the fin thickness. The fin height (H_f) is given by[60]

$$H_f = 0.75\left(\frac{D_i - d_o}{2}\right) \tag{73}$$

where D_i is the inner diameter of the heat exchanger annulus. Additionally, in eq 64, the overall surface efficiency (ξ_o) is given by

$$\xi_o = 1 - (1 - \xi_f)\frac{A_f}{A_t} \tag{74}$$

where the fin efficiency (ξ_f) is calculated using the equation

$$\xi_f = \tanh\left(\frac{m_f H_f}{m_f H_f}\right) \tag{75}$$

Here, m_f is given by[60]

$$m_f = \sqrt{\frac{2h_a}{k_{w,he}\delta_f}} \tag{76}$$

where h_a is the heat-transfer coefficient at the annulus side computed from eq 83, considering that Nu_a is given by eq 96. Then, to compute the inner (h_r) and outer (h_j) heat-transfer coefficients at the reactor, eqs 77 and 78 are used.[61]

$$Nu_r = 0.85 Re_r^{2/3} Pr_r^{1/3} \left(\frac{Z}{T}\right)^{-0.56} \left(\frac{D}{T}\right)^{0.13} \tag{77}$$

$$Nu_j = \begin{cases} 1.86\left(Re_j Pr_j \frac{D_{e,j}}{L_j}\right)^{1/3} \left(\frac{\mu_j}{\mu_{w,j}}\right)^{0.14} & Re_j \le 2300 \\ 0.027 Re_j^{4/5} Pr_j^{1/3} \left(\frac{\mu_j}{\mu_{w,j}}\right)^{0.14} & Re_j > 2300 \end{cases} \tag{78}$$

Here, D represents the impeller diameter. The equivalent diameter for heat transfer at the jacket ($D_{e,j}$) is given by

$$D_{e,j} = 2(D_{jo} - D_{ji}) \tag{79}$$

Also, the length of jacket passage (L_j) can be computed as

$$L_j = 2\pi r_c N_t \tag{80}$$

where the center-line jacket radius (r_c) is given by[61]

$$r_c = \frac{D_{jo} + D_{ji}}{4} \tag{81}$$

On the other hand, to compute the inner (h_t) and outer (h_a) heat-transfer coefficients at the heat exchanger, the following equations are used[60,62]

$$Nu_t = \begin{cases} 1.86\left(Re_t Pr \frac{d_i}{L_t}\right)^{1/3} & Re_t < 2300 \\ \frac{(f_t/2)(Re_t - 1000)Pr_t}{1 + 12.7(f_t/2)^{1/2}(Pr_t^{2/3} - 1)} & 2300 \le Re_t \le 10^4 \\ \frac{(f_t/2)Re_t Pr_t}{1 + 8.7(f_t/2)^{1/2}(Pr_t - 1)} & Re_t < 10^4 \end{cases} \tag{82}$$

dx.doi.org/10.1021/ie500587r | Ind. Eng. Chem. Res. XXXX, XXX, XXX−XXX

$$Nu_a = \begin{cases} 1.86\left(Re_a Pr_a \frac{D_h}{L_t}\right)^{1/3}\left(\frac{\mu_a}{\mu_{w,a}}\right)^{0.14} & Re_a < 2300 \\ \frac{(f_a/2)(Re_a - 1000)Pr_a}{1 + 12.7(f_a/2)^{1/2}(Pr_a^{2/3} - 1)} & 2300 \le Re_a \le 10^4 \\ \frac{(f_a/2)Re_a Pr_a}{1 + 8.7(f_a/2)^{1/2}(Pr_a - 1)} & Re_a < 10^4 \end{cases} \quad (83)$$

where the Fanning friction factors for the inner tube (f_t) and annulus (f_a) are given by[62]

$$f_t = \begin{cases} 0.079 Re_t^{-1/4} & 2300 \le Re_t \le 10^4 \\ \frac{1}{4}[1.82 \log(Re_t) - 1.64]^{-2} & Re_t < 10^4 \end{cases} \quad (84)$$

$$f_a = \begin{cases} 0.079 Re_a^{-1/4} & 2300 \le Re_t \le 10^4 \\ \frac{1}{4}[1.82 \log(Re_a) - 1.64]^{-2} & Re_t < 10^4 \end{cases} \quad (85)$$

In eqs 77−85, the Reynolds numbers at the reactor (Re_r), jacket (Re_j), annulus (Re_a), and inner tube (Re_t) can be computed using the equations

$$Re_r = \frac{D^2 N \rho_r}{\mu_r} \quad (86)$$

$$Re_j = \frac{D_{e,j}\rho_1 F_1}{A_{x,j}\mu_1} \quad (87)$$

$$Re_a = \frac{D_h \rho_2 F_2}{A_{x,a}\mu_2} \quad (88)$$

$$Re_t = \frac{d_i \rho_2 F_3}{A_{x,t}\mu_3} \quad (89)$$

The Prandtl numbers at the reactor (Pr_r), jacket (Pr_j), annulus (Pr_a), and inner tube (Pr_t) are calculated as

$$Pr_r = \frac{C_{p,r}\mu_r}{k_r} \quad (90)$$

$$Pr_j = \frac{C_{p,1}\mu_1}{k_1} \quad (91)$$

$$Pr_a = \frac{C_{p,2}\mu_2}{k_2} \quad (92)$$

$$Pr_t = \frac{C_{p,3}\mu_3}{k_3} \quad (93)$$

Also, in eqs 77− 83, the Nusselt numbers at the reactor (Nu_r), jacket (Nu_j), annulus (Nu_a), and inner tube (Nu_t) are given by[60,61]

$$Nu_r = \frac{h_r T}{k_r} \quad (94)$$

$$Nu_j = \frac{h_j D_{e,j}}{k_1} \quad (95)$$

$$Nu_a = \frac{h_a D_{e,a}}{k_2} \quad (96)$$

$$Nu_t = \frac{h_t d_i}{k_3} \quad (97)$$

In addition, in eqs 87−89, the cross-sectional flow areas at the jacket ($A_{x,j}$), annulus ($A_{x,a}$), and inner tube ($A_{x,t}$) are computed according to[60,61]

$$A_{x,j} = L\left(\frac{D_{jo} - D_{ji}}{2}\right) \quad (98)$$

$$A_{x,a} = \frac{\pi}{4}(D_i^2 - d_o^2) - H_f \delta_f N_f \quad (99)$$

$$A_{x,t} = \pi \frac{d_i^2}{4} \quad (100)$$

Here, L and N_{turns} represent the jacket fluid length and the number of fluid turns at the jacket, respectively. Also, in eq 88, D_h is the hydraulic diameter, given by

$$D_h = 4\frac{A_{x,a}}{P_w} \quad (101)$$

In eq 96, $D_{e,a}$ is the equivalent diameter for heat transfer at the annulus, computed as[60]

$$D_{e,a} = 4\frac{A_{x,a}}{P_h} \quad (102)$$

where the total wetted perimeter of the annulus (P_w) can be obtained as

$$P_w = \pi d_o(D_i + d_o) + 2H_f N_f \quad (103)$$

and the heat-transfer perimeter of the annulus (P_h) can be calculated from[60]

$$P_h = \pi d_o + 2H_f N_f \quad (104)$$

In eqs 33 and 34, volumes of the inner tube (V_t) and annulus (V_a) are given by[60]

$$V_t = A_{x,t} 2L_t N_{hp} \quad (105)$$

$$V_a = A_{x,a} 2L_t N_{hp} \quad (106)$$

In eqs 90 and 94, the reactor fluid thermal conductivity (k_r) is calculated as[49]

$$k_r = \phi_m k_m + \phi_p k_p + \phi_s k_s \quad (107)$$

where k_m, k_p, and k_s are the thermal conductivities of the monomer, polymer, and water, respectively. The cooling fluid thermal conductivities at the jacket input (k_1) and output (k_2) are given by[58]

$$k_1 = -2.429 \times 10^{-2} + 1.615 \times 10^{-3} T_1 - 1.912 \times 10^{-6} T_1^2 \quad (108)$$

$$k_2 = -2.429 \times 10^{-2} + 1.615 \times 10^{-3} T_2 - 1.912 \times 10^{-6} T_2^2 \quad (109)$$

dx.doi.org/10.1021/ie500587r | Ind. Eng. Chem. Res. XXXX, XXX, XXX−XXX

In addition, in eqs 86 and 90, the reactor fluid dynamic viscosity (μ_r) is given by

$$\mu_r = x_m\mu_m + x_p\mu_p + x_s\mu_s \tag{110}$$

where μ_m, μ_p, and μ_s are the dynamic viscosities of the monomer, polymer, and water, respectively. Here, the mole fractions of monomer (x_m), polymer (x_p) and water (x_w) are obtained from[51]

$$x_m = \frac{\frac{\phi_m\rho_m}{M_{w,m}}}{\frac{\phi_m\rho_m}{M_{w,m}} + \frac{\phi_p\rho_p}{M_w} + \frac{\phi_s\rho_s}{M_{w,s}}} \tag{111}$$

$$x_p = \frac{\frac{\phi_p\rho_p}{M_w}}{\frac{\phi_m\rho_m}{M_{w,m}} + \frac{\phi_p\rho_p}{M_w} + \frac{\phi_s\rho_s}{M_{w,s}}} \tag{112}$$

$$x_s = 1 - x_m - x_p \tag{113}$$

Here, μ_r is computed by means of the mole fraction of pure species because this property is highly dependent on the polymer molecular weight.[45,47]

The dynamic viscosities of the cooling fluid at the jacket input (μ_1) and output (μ_2) are computed using[58]

$$\mu_1 = 0.73439e^{-0.01663T_1} \tag{114}$$

$$\mu_2 = 0.73439e^{-0.01663T_2} \tag{115}$$

and those at the jacket wall ($\mu_{w,j}$) and at the annulus wall ($\mu_{w,a}$) are given by[58]

$$\mu_{w,j} = 0.73439e^{-0.01663T_{w,j}} \tag{116}$$

$$\mu_{w,a} = 0.73439e^{-0.01663T_{w,a}} \tag{117}$$

Here, the wall temperatures at the jacket ($T_{w,j}$) and annulus ($T_{w,a}$) are given by[60]

$$T_{w,j} = \frac{T_r + T_1}{2} \tag{118}$$

$$T_{w,a} = \frac{T_2 + T_3}{2} \tag{119}$$

The number-average (M_n) and weight-average (M_w) molecular weights are given by[50,63]

$$M_n = \frac{\lambda_1 + \eta_1}{\lambda_0 + \eta_0}M_{w,m} \tag{120}$$

$$M_w = \frac{\lambda_2 + \eta_2}{\lambda_1 + \eta_1}M_{w,m} \tag{121}$$

Because M_n and M_w are strongly related to the functional properties of the polymer such as particle size, impact strength, rigidity, tensile strength, chemical resistance, and thermal stability, among others,[45,50] this work seeks to maintain their values when scaling up the process. The solution of the previously presented coupled differential and algebraic equations was done in EMSO (Environment for Modeling, Simulation and Optimization).

4.2. Implementation of the Scaleup Procedure. As mentioned before, the previously presented model was reduced during the scaleup task. For model simplification, the following assumptions were considered:

- The dependency of the reactor fluid density on temperature is neglected; only the concentration dependency is considered, because the reactor temperature is controlled.[53,63]
- Kinetic constants k_d, k_I, k_{pg}, k_{fm}, k_t, k_{tc}, and k_{td} are evaluated at $T_{r,sp}$, given the reactor isothermal operation.[64]
- Given that the variations of $C_{p,r}$, μ_r, and k_r with concentration and temperature are small, these parameters are considered constant (average values) along the batch.[63,64]
- The quasi-steady-state approximation (QSSA) is applied to primary radicals (R) and the zeroth (λ_0), first (λ_1), and second (λ_2) moments of the live polymer chains.[63]
- T_1 is considered as a known input variable to the process, that is, its value at each stage of the batch is known.

The simplified model is composed of differential eqs 22, 24, and 28−32. Also, in eqs 23 and 25−27, the time dependence of each species is neglected, according to the QSSA for R, λ_0, λ_1, and λ_2, giving rise to eqs 122−125. These algebraic equations describe the behavior of these species during the batch.

$$R = \frac{2fk_dI}{k_IM} \tag{122}$$

$$\lambda_0 = \left(\frac{2fk_dI}{k_t}\right)^{1/2} \tag{123}$$

$$\lambda_1 = \lambda_0\left(1 + \frac{k_{pg}M}{k_{fm}M + k_t\lambda_0}\right) \tag{124}$$

$$\lambda_2 = \lambda_1\left(1 + \frac{2k_{pg}M}{k_{fm}M + k_t\lambda_0}\right) \tag{125}$$

Here, k_d, k_I, k_{pg}, k_{fm}, k_t, k_{tc}, and k_{td}, given by eqs 35−40, are evaluated at $T_{r,sp}$. Also, ρ_m and ρ_p, computed according to eqs 44 and 45, are evaluated at $T_{r,sp}$. The rest of the parameters involved in the simplified model (V_r, V_j, ρ_1, ρ_2, $C_{p,1}$, $C_{p,2}$, F_1, F_2, and $\dot{Q}_1$) are computed using the corresponding algebraic equations presented in the previous subsection. Also, as $\lambda_0 \ll \eta_0$, $\lambda_1 \ll \eta_1$, and $\lambda_2 \ll \eta_2$ (because they are highly reactive species), the number-average (M_n) and weight-average (M_w) molecular weights can be simplified to

$$M_n = \frac{\eta_1}{\eta_0}M_{w,m} \tag{126}$$

$$M_w = \frac{\eta_2}{\eta_1}M_{w,m} \tag{127}$$

Each one of the 13 steps of the procedure is performed as follows. The computational implementation was carried out using the MATLAB m-code programming language.

Step 1: $CV_{cs} = 0.1\ m^3$, $CV_{ns} = 1.5\ m^3$, and $\Delta CV = 0.1\ m^3$ are defined.

Step 2: A PBSM of the process is obtained. The PBSM composed of differential eqs 22, 24, and 28−32 describes the dynamic behavior of the reactor.

Step 3: **x**, **z**, **p**, and **w** are defined according to the model as follows

dx.doi.org/10.1021/ie500587r | Ind. Eng. Chem. Res. XXXX, XXX, XXX−XXX

$$\mathbf{x} = [I \quad M \quad \eta_0 \quad \eta_1 \quad \eta_2 \quad T_r \quad T_2] \tag{128}$$

$$\mathbf{z} = [V_{r,0} \quad T_1] \tag{129}$$

$$\mathbf{p} = [f \quad k_d \quad k_1 \quad k_{pg} \quad k_{fm} \quad k_{tc} \quad k_{td} \quad \Delta H_p \quad C_{p,r} \quad T_{ref} \quad M_{w,m} \quad \tau_j \quad \phi_{m,0} \quad M_0 \quad \rho_{r,0}] \tag{130}$$

$$\mathbf{w} = [V_r \quad V_j \quad F_1 \quad F_2 \quad U_r \quad A_r] \tag{131}$$

Step 4: The OT is fixed at the cs. Here, the OT is obtained by solving the process model considering that $T_r = 358.15 \pm 1$ K and including the effect of manipulating F_3 so the reactor fluid is able to reach this temperature range. Here, it is considered that the optimal OT occurs when T_r is set at 358.15 K,[45] where the polymerization can take place achieving the desired polymer molecular weight with minor risk of a thermal runaway.[41]

Intermediate steps a–f: These steps are followed to compute the $SII_{x_{k,cs}}$.

(a) An expression for each $w_i|_{cs} = f(\mathbf{z_{cs}})$ must be found. Thus, V_r is calculated by eq 67, V_j by eq 68, F_2 by eq 50, U_r by eq 63, A_r by eq 65, and F_1 by the equation

$$F_1 = \frac{V_j}{\tau_j} \tag{132}$$

where τ_j is the residence time for the cooling fluid at the jacket input.

(b) The model is linearized along the OT according to eqs 3 and 4.

(c) Matrices $\mathbf{B}_c$ and $\mathbf{C}_c$ are modified using eqs 5 and 6, considering that $y_{i,min}$ and $y_{i,max}$ are the minimum and maximum values, respectively, of each y_i during the batch at the cs, because minor changes are expected for these limits at the cs. Here, $T_{1,min}$ and $T_{1,max}$ also are the minimum and maximum values, respectively, of T_1 and $V_{r,0}$ limits are computed as the ±10% of its nominal value at the cs.

(d) The model is discretized using $t_s = 120$ s. Here, t_s must be small to represent each continuous linear model. For this case, it was chosen to be equal to the time step for constructing the ensemble of continuous linear models. Given the slow nature of BPs,[4,40] if t_s is changed (to a consistent value), the dynamics hierarchy is not altered.

(e) The $\boldsymbol{\mathcal{O}}$, $\boldsymbol{\mathcal{C}}$, and $\boldsymbol{\mathcal{H}}$ matrices are computed from eqs 9–11, where $n = 7$, $m = n = 7$, and $p = 2$.

(f) $\boldsymbol{\mathcal{H}}$ is decomposed into singular values using eq 12.

Step 5: $SII_{x_{k,cs}}$ is computed using 13 with $\text{rank}(\boldsymbol{\mathcal{H}}) = r = 2$. Figure 3 shows the $SII_{x_{k,cs}}$ profiles, where it can be seen that $SII_{T_r} > SII_{T_2} > \{SII_I, SII_M, SII\eta_0, SII\eta_1, SII\eta_2\}$.

According to this, T_r is the most impacted dynamics by the design variables of the process. Here, it is worth clarifying that the SII curves can be affected by the controller tuning, so the designer must be careful to properly tune the controller because, by using the proposed methodology, the OT at the cs is transferred to the ns and, if the controller is poorly tuned, an oversized unit might be designed at the cs, instead of the actually required one.

Step 6: The critical point of the batch is identified. It corresponds to $SII_{T_r,cs} = 4.97$ at $t = 5$ h as can be seen in Figure 3.

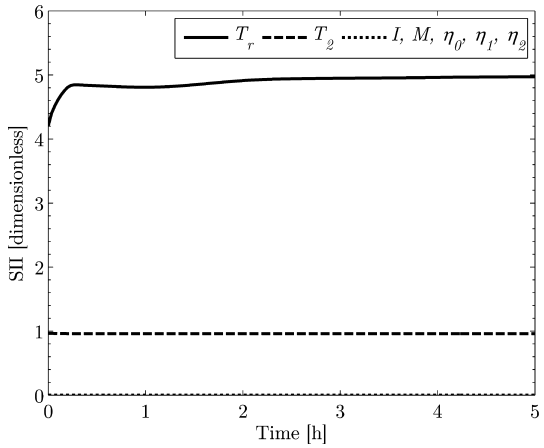

Figure 3. State impactability index at the cs.

Step 7: This point is selected as the RP for scaling up the process. Values for the state variables at the RP are reported in Table 1.

Table 1. RP for Scaling up the Process

variable	value	SI units
I	9.56×10^{-4}	kmol/m^3
M	3.75×10^{-1}	kmol/m^3
η_0	6.33×10^{-3}	kmol/m^3
η_1	2.19×10^{0}	kmol/m^3
η_2	1.67×10^{3}	kmol/m^3
T_r	358.14	K
T_2	357.41	K

Intermediate Steps i–vi: These steps are followed to determine $SII_{x_{k,RP}}$ as the scale is increased.

(i) An expression for each $w_i|_{RP} = f(\mathbf{z_{RP}})$ is found. Considering that eq 63 fixes the given geometry of the reactor, two cases for the overall heat-transfer coefficient are considered: available ($U_{r,a}$) and required ($U_{r,r}$). For the former, eq 63 is used for computing $U_{r,a}$, and for the latter, $U_{r,r}$ is computed as

$$U_{r,r} = -\frac{F_1 C_{p,1}|_{RP} \rho_1|_{RP} (T_1|_{RP} - T_{ref}) - F_2 C_{p,2}|_{RP} \rho_2|_{RP} (T_2|_{RP} - T_{ref})}{A_r (T_r|_{RP} - T_2|_{RP})} \tag{133}$$

where $U_{r,r}$ is evaluated at the RP. In addition, considering that most of the traditional scaleup methods involve the fulfillment of geometrical similarity, this comparison allows one to determine the effect of designing a unit geometrically similar instead of the required one. Notice that, in the first case, the process is scaled up keeping the overall heat-transfer coefficient fixed by the current scale design. In contrast, in the second case, the overall heat-transfer coefficient is computed from the process energy requirements without fixing the geometry of the reactor, making eq 133 valid when the scale is increased.

(ii) The model is linearized around the RP.

(iii) Matrices $\mathbf{B}_c$ and $\mathbf{C}_c$ are modified according to eqs 5 and 6, considering that the limits of y_i are the same as those set at the cs, because minor changes are expected for these limits when the scale is increased because the process dynamic behavior is transferred from the cs to the ns using this methodology. Here, the limits of T_1 also are equal to those set

dx.doi.org/10.1021/ie500587r | Ind. Eng. Chem. Res. XXXX, XXX, XXX–XXX

at the cs, and the limits of $V_{r,0}$ are computed as ±10% of its nominal value at each scale.

(iv) The linear model at the RP is discretized as shown in eqs 7 and 8 as the scale is increased, with t_s = 120 s. Here, it is also expected that each discrete model represents each continuous one at the RP.

(v) $\boldsymbol{O}$, $\boldsymbol{C}$, and $\boldsymbol{\mathcal{H}}$ are computed at the RP at each scale, using 9−11.

(vi) $\boldsymbol{\mathcal{H}}$ is decomposed in singular values as shown in eq 12.

Step 8: $SII_{x_{k,RP}}$ is computed from eq 13, where the Hankel matrix rank is r = 2.

Step 9: As can be seen from Figure 1, steps 5−12 are repeated until CV = CV_{ns}.

Step 10: The $SII_{x_{k,RP}}$ values are compared at the cs and ns, as can be seen from Table 2. Here, the SII values remain constant

Table 2. $SII_{x_{k,RP}}$ Values at the cs and ns

variable	SII_{cs}	$SII_{ns}\|_{U_{r,r}}$	$SII_{ns}\|_{U_{r,a}}$
I	0.00	0.00	0.00
M	0.00	0.00	0.00
η_0	0.00	0.00	0.00
η_1	0.00	0.00	0.00
η_2	0.00	0.00	0.00
T_r	4.97	4.97	3.35
T_2	0.96	0.96	0.98

when the process is scaled up when the energy requirements are constrained ($U_{r,r}$), and they change when geometrical similarity is held ($U_{r,a}$). This fact indicates that the process behavior deteriorates when $U_{r,a}$ is used during the scaleup.

In addition, the $\mathbf{w}|_{RP}$ values for all cases are reported in Table 3. It can be seen that a smaller value for the overall heat-transfer

Table 3. $\mathbf{w}_{RP}$ values at the cs and ns

variable	$\mathbf{w}_{cs}$	$\mathbf{w}_{ns}\|_{U_{r,r}}$	$\mathbf{w}_{ns}\|_{U_{r,a}}$	SI units
V_r	8.96×10^{-2}	1.34×10^{0}	1.34×10^{0}	m^3
V_j	3.61×10^{-2}	5.41×10^{-1}	5.41×10^{-1}	m^3
F_1	3.56×10^{0}	5.34×10^{1}	5.34×10^{1}	m^3/h
F_2	3.56×10^{0}	5.34×10^{1}	5.34×10^{1}	m^3/h
$U_r\|_{RP}$	2.45×10^{2}	6.05×10^{2}	3.40×10^{2}	W/(m^2 K)
A_r	7.68×10^{-1}	4.67×10^{0}	4.67×10^{0}	m^2

coefficient was computed when using $U_{r,a}$ than when using $U_{r,r}$; this means that a smaller process unit than required was designed.

Step 11: Given that values for each $w_i|_{RP}$ were determined at the ns (see Table 3), to obtain the exact scaled unit design that matches each $w_i|_{RP}$ requirement, an equation for each $w_i|_{ns}$ = $f(\mathbf{z}_{ns})$ is established. Therefore, taking into account that fact that only eq 133 satisfies the scaleup requirements (see Table 2), two cases are considered to fulfill $U_{r,r}$: (i) increasing the flow rate of the cooling fluid at the jacket input and (ii) setting a new jacket geometry. For the first case, F_1 is changed from 53.4 to 159 m^3/h to increase $U_{r,a}$ to the desired value. For the second case, three internal baffles are added to the jacket, using eq 134[61] instead of eq 78, to satisfy the heat-transfer demand ($U_{r,r}$) in the RP at the ns. From here, $U_{r,r}$ is computed using eq 63 for the baffles case, with Nu_j is given by eq 134 where h_j is computed according to eq 95.

$$Nu_j = \begin{cases} 1.86\left(Re_j Pr_j \dfrac{D_{e,j}}{L_j}\right)^{1/3}\left(\dfrac{\mu_j}{\mu_{w,j}}\right)^{0.14} & Re_j \le 2300 \\ 0.027 Re_j^{4/5} Pr_j^{1/3}\left(\dfrac{\mu_j}{\mu_{w,j}}\right)^{0.14} & Re_j > 2300 \\ \left(1 + 3.5\dfrac{D_{e,j}}{2r_c}\right) & \end{cases} \quad (134)$$

Step 12: The process is simulated with the values of $\mathbf{p}$, $\mathbf{z}_{ns}$, and $\mathbf{w}_{ns}$.

Intermediate Steps a−f: These steps are followed to compute $SII_{x_{k,ns}}$.

Step 13: $SII_{x_{k,ns}}$ is computed using eq 13. In this way, values of this index for the main dynamics (T_r) at each scale are compared in Figure 4. It can be seen that the SII_{T_r} profile for

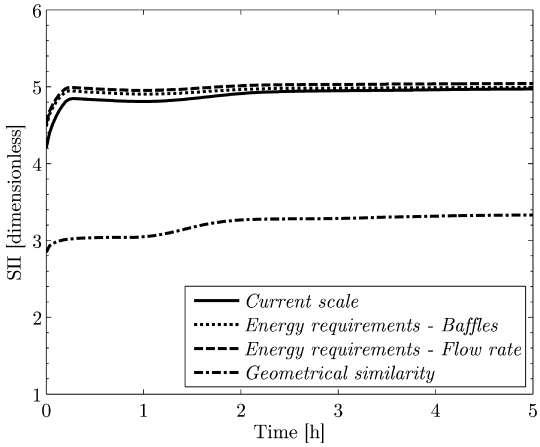

Figure 4. State impactability index at the ns for T_r.

the geometrical similarity case is highly different from the cs profile. Consequently, it is not possible to reproduce the same dynamic behavior of the reactor at the ns by maintaining geometrical similarity. Figure 4 also shows that there is little difference between the SII_{T_r} curves at the cs and ns for the baffles case; this difference is because the jacket must be designed with an integer number of baffles. Here, three baffles were added to the annular jacket, but the real requirement was for 2.8 units. Therefore, the overall heat-transfer coefficient in the reactor increased from 605 to 611 W/(m^2 K), decreasing the F_3 demand.

Also, from Figure 4, it can be seen that there is a small difference between the SII_{T_r} profiles at the cs and ns for the flow rate case. This effect is because, although the flow rate of cooling fluid at the jacket input satisfies the energy requirements at the end of the batch [$U_{r,r}$ = 605 W/(m^2 K)], it also has a greater cooling capacity from the process start, causing less energetic requirements at the heat exchanger throughout the batch and, hence, decreasing the flow rate needed at the heat exchanger to hold T_r = 358.15 K.

4.3. Comparison of the Proposed Methodology to a Traditional Method. To verify the process dynamic behavior at the ns, in this subsection, the complete model, composed of eqs 20−121, is used to simulate both units designs. In Figure 5, the dynamic evolutions of M_n and M_w for all cases are compared. It can be seen that there is difference between M_n

dx.doi.org/10.1021/ie500587r | Ind. Eng. Chem. Res. XXXX, XXX, XXX−XXX

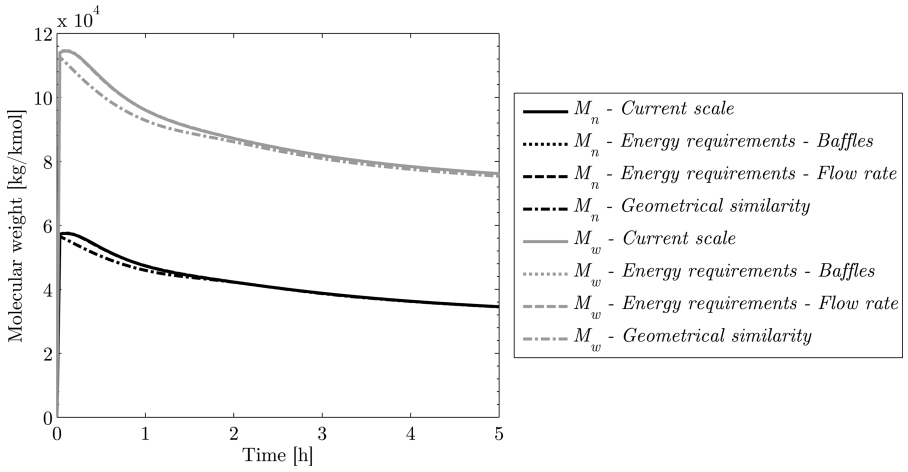

Figure 5. M_n and M_w at the cs and ns using the complete model.

and M_w at the cs and ns for the geometrical similarity case. This difference is because, when the process was scaled up using $U_{r,a}$, a smaller process unit was designed than required, causing that the reactor temperature (T_r) to increase at the beginning of the batch (see Figure 6), which elevates the values of the kinetic constants (k_d, k_I, k_{pg}, k_{fm}, k_t, k_{tc}, and k_{td}) and, hence, increases the termination rates to produce shorter polymer chains.

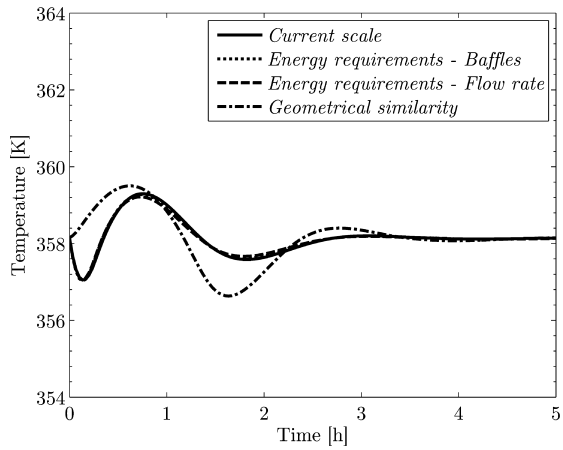

Figure 6. Comparison of T_r at the cs and ns using the complete model.

In Figure 5, it can also be seen that the curves for M_n and M_w at the cs and ns overlap for both cases when the energy requirements are held. This fact demonstrates that the process reaches the same quality targets at the ns from the cs when the proposed procedure is used. Also, a comparison of the reactor temperature dynamics (T_r) for all cases is shown in Figure 6.

Here, the same controller parameters are used for all cases. Figure 6 shows that the profiles of the energy requirements overlap with the cs profile. Also, it can be noticed that there is a difference between the geometrical similarity case and the cs profile. The same difference can be seen in Figure 7, where a comparison of the dynamic responses of the control input, namely, the cooling fluid flow rate at the inner tube input (F_3), for all cases is presented.

It can be seen that, when the process is scaled up with the geometrical similarity maintained, the flow rate reaches its maximum value during the first hour of polymerization. During this time, any disturbance introduced into the process cannot

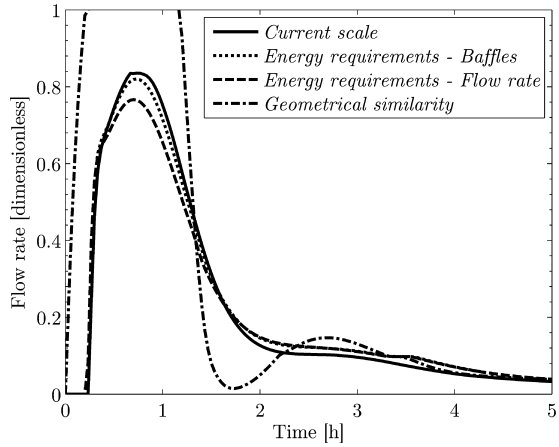

Figure 7. Comparison of F_3 at the cs and ns using the complete model.

be countered by the controller. Here, it is even clearer that the unit has a smaller size than required. In addition, the difference for the baffles case and the cs, as mentioned before, is due to the addition of three baffles instead of 2.8, and the difference for the flow rate case is due to the increment of the cooling capacity from the process start, as also mentioned before.

5. CONCLUSIONS

The main contribution of this work is the integration of an index (SII) into the scaleup of batch reactors, which allows the establishment of the real scale factors of a process maintaining the same dynamics hierarchy when changing the scale and, hence, determining whether two or more designed units can carry out the same process with the same performance targets. Here, the use of a process PBSM and its Hankel matrix to analyze the process dynamic behavior and scale it up, considering the effects of the design variables ($\mathbf{z}$) as a whole on each state variable (x_k), is the key for carrying out a successful scaleup.

A batch polymerization reactor was scaled up from 0.1 to 1.5 m^3. As a result, the scale factors for keeping the same polymer molecular weight trajectory at both scales were found. Here, it was established that the dynamics that was impacted most by the design variables was the reactor temperature (T_r) and the less impacted ones were the species concentrations (I, M, η_0, η_1, η_2). In addition, considering that traditional scaleup methods

dx.doi.org/10.1021/ie500587r | Ind. Eng. Chem. Res. XXXX, XXX, XXX−XXX

involve the fulfillment of geometrical similarity, from this example, it is shown that traditional scaleup methods do not always wind up with a good industrial unit design, and if the geometrical similarity is held, other parameters of the process need to be changed to achieve the same performance targets as set at the current scale of an industrial unit. Also, it is shown that, by means of SII calculations, it is possible to identify whether a process unit is over- or undersized.

AUTHOR INFORMATION

Corresponding Author

*E-mail: hdalvare@unal.edu.co. Tel.: +57 (4) 4255332. Fax: +57 (4) 2341002.

Notes

The authors declare no competing financial interest.

NOMENCLATURE

Latin Letters

$\mathbf{A}$ = system matrix
A_f = area of a fin (m^2)
A_i = inside area of the inner tube (m^2)
A_r = reactor transfer area (m^2)
A_t = overall outside area of the inner tube (m^2)
A_u = outside area of the inner tube (m^2)
A_x = cross-sectional flow area (m^2)
$\mathbf{B}$ = input matrix
$\mathbf{C}$ = output matrix
$\boldsymbol{C}$ = controllability matrix
$C_{p,i}$ = specific heat capacity of the ith stream [kJ/(kg K)]
$C_{p,m}$ = specific heat capacity of the monomer [kJ/(kg K)]
$C_{p,p}$ = specific heat capacity of the polymer [kJ/(kg K)]
$C_{p,r}$ = specific heat capacity of the reactor fluid [kJ/(kg K)]
$C_{p,s}$ = specific heat capacity of the water [kJ/(kg K)]
D = impeller diameter (m)
D_e = equivalent diameter (m)
D_h = hydraulic diameter (m)
d_i = inside diameter of the heat-exchanger inner tube (m)
D_i = inner diameter of heat-exchanger annulus (m)
D_{ij} = inner diameter of the annular jacket (m)
d_o = outside diameter of the heat-exchanger inner tube (m)
D_α = concentration of the dead polymer of α monomers ($kmol/m^3$)
D_β = concentration of the dead polymer of β monomers ($kmol/m^3$)
$\mathcal{F}$ = vector of state variable functions
f = initiator efficiency
f_a = fanning friction factor at the annulus
F_i = flow rate of the ith stream (m^3/s)
f_t = fanning friction factor at the inner tube
$\mathcal{G}$ = vector of output variable functions
$\mathcal{H}$ = Hankel matrix
h = heat-transfer coefficient [$W/(m^2 K)$]
H_f = fin height (m)
I = initiator concentration ($kmol/m^3$)
j = discrete time
K_D = derivative controller gain
k_d = decomposition kinetic constant (1/min)
k_{fm} = kinetic constant for chain transfer to polymer [m^3/(min kmol)]
K_I = integral controller gain
k_I = initiation kinetic constant [m^3/(min kmol)]
k_i = thermal conductivity of the ith stream [W/(m K)]
k_m = monomer thermal conductivity [W/(m K)]
K_P = proportional controller gain
k_p = polymer thermal conductivity [W/(m K)]
k_{pg} = propagation kinetic constant [m^3/(min kmol)]
k_r = reactor fluid thermal conductivity [W/(m K)]
k_s = water thermal conductivity [W/(m K)]
k_t = termination kinetic constant [m^3/(min kmol)]
k_{tc} = kinetic constant for termination by recombination [m^3/(min kmol)]
k_{td} = kinetic constant for termination by disproportionation [m^3/(min kmol)]
$k_{w,he}$ = heat-exchanger pipe thermal conductivity [W/(m K)]
$k_{w,r}$ = reactor wall thermal conductivity [W/(m K)]
L = jacket fluid length (m)
L_j = length of the jacket passage (m)
L_t = nominal length of the exchange section (m)
M = monomer concentration ($kmol/m^3$)
m = dimension of the vector of output variables
M_0 = initial monomer concentration ($kmol/m^3$)
m_f = coefficient for the fin efficiency calculation
M_n = number-average molecular weight (kg/kmol)
M_w = weight-average molecular weight (kg/kmol)
n = dimension of the vector of state variables
N_f = number of fins
N_{hp} = number of hairpins
N_{turns} = number of fluid turns at the jacket
Nu = Nusselt number
$\boldsymbol{O}$ = observability matrix
p = dimension of the vector of input variables
$\mathbf{p}$ = vector of synthesis parameters
P_α = concentration of the live polymer of α monomers ($kmol/m^3$)
P_β = concentration of the live polymer of β monomers ($kmol/m^3$)
P_h = heat-transfer perimeter of the annulus (m)
P_w = total wetted perimeter of the annulus (m)
Pr = Prandtl number
$\dot{Q}_1$ = heat-transfer rate at the reactor (W)
$\dot{Q}_2$ = heat-transfer rate at the double-pipe heat exchanger (W)
R = concentration of primary radicals ($kmol/m^3$)
r = matrix rank
r_c = center-line radius (m)
R_{fi} = inner-tube fouling resistance (m^2 K/W)
R_{fo} = annulus fouling resistance (m^2 K/W)
R_g = ideal gas constant [cal/(mol K)]
Re = Reynolds number
SII = state impactability index
T = tank diameter (m)
t = time
T_i = temperature of the ith stream (K)
T_r = reactor temperature (K)
T_w = fluid wall temperature (K)
$\mathbf{U}$ = SVD matrix composed by left singular vectors
U_{he} = overall heat-transfer coefficient at the heat exchanger [$W/(m^2 K)$]
U_r = overall heat-transfer coefficient at the reactor [$W/(m^2 K)$]
$\mathbf{V}$ = SVD matrix composed by the right singular vectors
V_a = volume of the annulus [m^3]
V_{bottom} = volume of the reactor bottom [m^3]
V_j = jacket volume [m^3]
V_r = reactor volume [m^3]

dx.doi.org/10.1021/ie500587r | Ind. Eng. Chem. Res. XXXX, XXX, XXX−XXX

$V_{r,0}$ = initial reactor volume [m^3]
V_t = volume of the inner tube [m^3]
w = vector of design-variable-dependent parameters
x = vector of state variables
X_m = monomer conversion
x_m = monomer mole fraction
x_p = polymer mole fraction
x_s = water mole fraction
y = vector of output variables
Z = reactor fluid height (m)
z = vector of design variables

Greek Letters

δ_f = fin thickness (m)
ΔH_p = heat of polymerization (J/kmol)
ϵ = contraction factor
η_0 = zeroth moment of the dead polymer chains (kmol/m^3)
η_1 = first moment of the dead polymer chains (kmol/m^3)
η_2 = second moment of the dead polymer chains (kmol/m^3)
λ_0 = zeroth moment of the live polymer chains (kmol/m^3)
λ_1 = first moment of the live polymer chains (kmol/m^3)
λ_2 = second moment of the live polymer chains (kmol/m^3)
μ_i = fluid dynamic viscosity of the ith stream (Pa s)
μ_m = monomer fluid dynamic viscosity (Pa s)
μ_p = polymer fluid dynamic viscosity (Pa s)
μ_r = reactor fluid dynamic viscosity (Pa s)
μ_s = water fluid dynamic viscosity (Pa s)
μ_w = fluid wall dynamic viscosity (Pa s)
ξ_f = fin efficiency
ξ_o = overall surface efficiency
ρ_i = fluid density of the ith stream (kg/m^3)
ρ_m = monomer density (kg/m^3)
ρ_p = polymer density (kg/m^3)
ρ_r = reactor fluid density (kg/m^3)
$\rho_{r,0}$ = initial reactor fluid density (kg/m^3)
σ_{ii} = ith singular value
$\mathbf{\Sigma}$ = matrix of singular values
ϕ_m = volume fraction of monomer
$\phi_{m,0}$ = initial volume fraction of monomer
ϕ_p = volume fraction of polymer
ϕ_s = volume fraction of water

Subscripts

0 = initial condition
a = annulus fluid side
c = continuous system
d = discrete system
j = jacket fluid side
max = maximum value
min = minimum value
N = nominal value
r = reactor fluid side
t = inner tube fluid side
sp = set point

Superscript

T = matrix transpose

Abbreviations

BP = batch process
CP = continuous process
cs = current scale
CV = capacity variable
ns = new scale
OR = operating regime
OT = operating trajectory
PBSM = phenomenological-based semiphysical model
RP = reference point
SVD = singular value decomposition

REFERENCES

(1) Fernández, I.; Renedo, C. J.; Pérez, S. F.; Ortiz, A.; Mañana, M. A Review: Energy Recovery in Batch Processes. *Renewable Sustainable Energy Rev.* **2012**, *16*, 2260−2277.
(2) Stephanopoulos, G.; Ali, S.; Linninger, A.; Salomone, E. Batch Process Development: From Reactions to Manufacturing Systems. *Comput. Chem. Eng.* **1999**, *23* (Suppl.), S975−S984.
(3) Donati, G.; Paludetto, R. Batch and Semibatch Catalytic Reactors (From Theory to Practice). *Catal. Today* **1999**, *52*, 183−195.
(4) Bonvin, D. Optimal Operation of Batch Reactors—A Personal View. *J. Process Control* **1998**, *8*, 355−368.
(5) Towler, G.; Sinnott, R. *Chemical Engineering Design*, 2nd ed.; Butterworth-Heinemann: Boston, 2013; pp 631−751.
(6) Shaikh, A.; Al-Dahhan, M. Scale-up of Bubble Column Reactors: A Review of Current State-of-the-Art. *Ind. Eng. Chem. Res.* **2013**, *52*, 8091−8108.
(7) Knowlton, T. M.; Karri, S. B. R.; Issangya, A. Scale-up of Fluidized-Bed Hydrodynamics. *Powder Technol.* **2005**, *150*, 72−77.
(8) Caygill, G.; Zanfir, M.; Gavriilidis, A. Scalable Reactor Design for Pharmaceuticals and Fine Chemicals Production 1: Potential Scale-up Obstacles. *Org. Process Res. Dev.* **2006**, *10*, 539−552.
(9) Ruiz, A. A.; Alvarez, H. Scale-up of Chemical and Biochemical Processes Using a Phenomenological Model. *Inf. Tecnol.* **2011**, *22*, 33−52 (in Spanish).
(10) Rüdisüli, M.; Schildhauer, T. J.; Biollaz, S. M. A.; van Ommen, J. R. Scale-up of Bubbling Fluidized Bed Reactors—A Review. *Powder Technol.* **2012**, *217*, 21−38.
(11) Ruzicka, M. C. On Dimensionless Numbers. *Chem. Eng. Res. Des.* **2008**, *86*, 835−868.
(12) Sweere, A. P. J.; Luyben, K. C. A. M.; Kossen, N. W. F. Regime Analysis and Scaledown: Tools to Investigate the Performance of Bioreactors. *Enzyme Microb. Technol.* **1987**, *9*, 386−398.
(13) Meyer, T. Scale-up of Polymerization Process: A Practical Example. *Org. Process Res. Dev.* **2003**, *7*, 297−302.
(14) Gasparini, G.; Archer, I.; Jones, E.; Ashe, R. Scaling up Biocatalysis Reactions in Flow Reactors. *Org. Process Res. Dev.* **2012**, *16*, 1013−1016.
(15) Garcia-Ochoa, F.; Gomez, E. Bioreactor Scale-up and Oxygen Transfer Rate in Microbial Processes: An Overview. *Biotechnol. Adv.* **2009**, *27*, 153−176.
(16) Ranade, V. V.; Chaudhari, R. V.; Gunjal, P. R. *Trickle Bed Reactors: Reactor Engineering & Applications*; Elsevier: Amsterdam, 2011; pp 171−210.
(17) Ehly, M.; Gemperline, P. J.; Nordon, A.; Littlejohn, D.; Basford, J. K.; De Cecco, M. Scale-up of Batch Kinetic Models. *Anal. Chim. Acta* **2007**, *595*, 80−88.
(18) Pollard, D. J.; Kirschner, T. F.; Hunt, G. R.; Tong, I. T.; Stieber, R.; Salmon, P. M. Scale-up of a Viscous Fungal Fermentation: Application of Scale-up Criteria with Regime Analysis and Operating Boundary Conditions. *Biotechnol. Bioeng.* **2007**, *96*, 307−317.
(19) Fathi Roudsari, S.; Ein-Mozaffari, F.; Dhib, R. Use of CFD in Modeling MMA Solution Polymerization in a CSTR. *Chem. Eng. J.* **2013**, *219*, 429−442.
(20) Vargas, R. O.; López-Serrano, F. *Experimental and Computational Fluid Mechanics*; Springer International Publishing: New York, 2014; pp 235−241.
(21) Hickman, D. A.; Holbrook, M. T.; Mistretta, S.; Rozeveld, S. J. Successful Scale-up of an Industrial Trickle Bed Hydrogenation Using Laboratory Reactor Data. *Ind. Eng. Chem. Res.* **2013**, *52*, 15287−15292.
(22) Lonsane, B. K.; Saucedo-Castaneda, G.; Raimbault, M.; Roussos, S.; Viniegra-Gonzalez, G.; Ghildyal, N. P.; Ramakrishna, M.; Krishnaiah, M. M. Scale-up Strategies for Solid State Fermentation Systems. *Process Biochem.* **1992**, *27*, 259−273.

(23) Leckner, B.; Szentannai, P.; Winter, F. Scale-up of Fluidized-Bed Combustion—A Review. *Fuel* **2011**, *90*, 2951−2964.
(24) Bisio, A.; Kabel, R. L. *Scaleup of Chemical Processes: Conversion from Laboratory Scale Tests to Successful Commercial Size Design*; John Wiley & Sons, Inc.: New York, 1985; p 699.
(25) Dudukovic, M. P. Reaction Engineering: Status and Future Challenges. *Chem. Eng. Sci.* **2010**, *65*, 3−11.
(26) Gavi, E.; Marchisio, D. L.; Barresi, A. A. CFD Modelling and Scale-up of Confined Impinging Jet Reactors. *Chem. Eng. Sci.* **2007**, *62*, 2228−2241.
(27) Leuenberger, H. New Trends in the Production of Pharmaceutical Granules: The Classical Batch Concept and the Problem of Scale-up. *Eur. J. Pharm. Biopharm.* **2001**, *52*, 279−288.
(28) Alvarez, H.; Lamanna, R.; Revollar, S. Methodology for Obtaining Phenomenological-Based Semiphysical Models Applied to a Sugar Cane Sulphitation Process. *Rev. Iberoam. Autom. Inf. Ind.* **2009**, *6*, 10−20 (in Spanish).
(29) Choo, Y. On the Property of a Discrete Impulse Response Gramian with Application to Model Reduction. *IEICE Trans. Fundam. Electron. Commun. Comput. Sci.* **2005**, *E88-A*, 3658−3660.
(30) Yin, H.; Zhu, Z.; Ding, F. Model Order Determination Using the Hankel Matrix of Impulse Responses. *Appl. Math. Lett.* **2011**, *24*, 797−802.
(31) Álvarez, L. A. Design Methodology for Plantwide Control. Master's Thesis, Universidad Nacional de Colombia, Medellín, Colombia, 2008 (in Spanish).
(32) Inglezakis, V. J.; Poulopoulos, S. G. *Adsorption, Ion Exchange and Catalysis: Design of Operations and Environmental Applications*; Elsevier: Amsterdam, 2006; pp 523−550.
(33) Monsalve-Bravo, G. M.; Moscoso-Vasquez, H. M.; Alvarez, H. Scale-up of Continuous Reactors Using Phenomenological-Based Models. *Chim. Oggi−Chem. Today*, in press.
(34) Coker, A. K. *Modeling of Chemical Kinetics and Reactor Design*; Gulf Professional Publishing: Houston, TX, 2001; pp 1034−1081.
(35) Zlokarnik, M. *Scale-up in Chemical Engineering*, 2nd ed.; Wiley-VCH Verlag GmbH & Co. KGaA: Weinheim, Germany, 2006; p 271.
(36) Donati, G.; Paludetto, R. Scale-up of Chemical Reactors. *Catal. Today* **1997**, *34*, 483−533.
(37) Nikakhtari, H.; Song, W.; Nemati, M.; Hill, G. A. Oxygen Mass Transfer and Scale-up Studies in Baffled Roller Bioreactors. *Bioprocess. Biosyst. Eng.* **2014**, *37*, 193−203.
(38) Anderson, N. Practical Use of Continuous Processing in Developing and Scaling up Laboratory Processes. *Org. Process Res. Dev.* **2001**, *5*, 613−621.
(39) Lee, K. S.; Lee, J. H. Iterative Learning Control-Based Batch Process Control Technique for Integrated Control of End Product Properties and Transient Profiles of Process Variables. *J. Process Control* **2003**, *13*, 607−621.
(40) Bonvin, D.; Srinivasan, B.; Hunkeler, D. Control and Optimization of Batch Processes. *IEEE Control Syst. Mag.* **2006**, *26*, 34−45.
(41) Westerterp, K. R.; Molga, E. J. Safety and Runaway Prevention in Batch and Semibatch Reactors—A Review. *Chem. Eng. Res. Des.* **2006**, *84*, 543−552.
(42) Kalman, R. E. On the General Theory of Control Systems. *IRE Trans. Autom. Control* **1959**, *4*, 110.
(43) Antoulas, A. C. An Overview of Approximation Methods for Large-Scale Dynamical Systems. *Annu. Rev. Control* **2005**, *29*, 181−190.
(44) Vivaldo-Lima, E.; Wood, P. E.; Hamielec, A. E.; Penlidis, A. An Updated Review on Suspension Polymerization. *Ind. Eng. Chem. Res.* **1997**, *36*, 939−965.
(45) Yuan, H. G.; Kalfas, G.; Ray, W. H. Suspension Polymerization. *Polym. Rev.* **1991**, *31*, 215−299.
(46) Langner, F.; Moritz, H. U.; Reichert, K. H. Reactor Scale-up for Polymerization in Suspension. *Chem. Eng. Sci.* **1980**, *35*, 519−525.
(47) Brooks, B. W. Suspension Polymerization Processes. *Chem. Eng. Technol.* **2010**, *33*, 1737−1744.
(48) Achilias, D. S. A Review of Modeling of Diffusion Controlled Polymerization Reactions. *Macromol. Theory Simul.* **2007**, *16*, 319−347.
(49) Louie, B. M.; Carratt, G. M.; Soong, D. S. Modeling the Free Radical Solution and Bulk Polymerization of Methyl Methacrylate. *J. Appl. Polym. Sci.* **1985**, *30*, 3985−4012.
(50) Rivera-Toledo, M.; Flores-Tlacuahuac, A.; Vílchis-Ramírez, L. Dynamic Optimization of the Methyl Methacrylate Cell-Cast Process for Plastic Sheet Production. *AIChE J.* **2009**, *55*, 1464−1486.
(51) Zhou, F.; Guptam, S. K.; Ray, A. K. Modeling of the Sheet-Molding Process for Poly(methyl methacrylate). *J. Appl. Polym. Sci.* **2001**, *81*, 1951−1971.
(52) Crowley, T. J.; Choi, K. On-Line Monitoring and Control of a Batch Polymerization Reactor. *J. Process Control* **1996**, *6*, 119−127.
(53) Santos, J. C.; Lopes, C. N.; Reis, M. M.; Giudici, R.; Sayer, C.; Machado, R. A. F.; Araújo, P. H. H. Comparison of Techniques for the Determination of Conversion during Suspension Polymerization Reactions. *Braz. J. Chem. Eng.* **2008**, *25*, 399−407.
(54) Cherbański, R.; Milewska, A.; Molga, E. Safety Aspects in Batch Reactors for Styrene Suspension Polymerization. *Ind. Eng. Chem. Res.* **2007**, *46*, 5898−5906.
(55) Shahrokhi, M.; Fanaei, M. A. Nonlinear Temperature Control of a Batch Suspension Polymerization Reactor. *Polym. Eng. Sci.* **2002**, *42*, 1296−1308.
(56) Saliakas, V.; Chatzidoukas, C.; Krallis, A.; Meimaroglou, D.; Kiparissides, C. Dynamic Optimization of Molecular Weight Distribution Using Orthogonal Collocation on Finite Elements and Fixed Pivot Methods: An Experimental and Theoretical Investigation. *Macromol. React. Eng.* **2007**, *1*, 119−136.
(57) Saliakas, V.; Kotoulas, C.; Meimaroglou, D.; Kiparissides, C. Dynamic Evolution of the Particle Size Distribution in Suspension Polymerization Reactors: A Comparative Study on Monte Carlo and Sectional Grid Methods. *Can. J. Chem. Eng.* **2008**, *86*, 924−936.
(58) Dow Chemical Company Products Material Safety Data Sheet Page, Material Safety Data Sheet of the Tetraethylene Glycol. http://www.dow.com (accessed Nov 10, 2013).
(59) Reklaitis, G. V.; Schneider, D. R. *Introduction to Material and Energy Balances*; Wiley: New York, 1986; p 683.
(60) Kakaç, S.; Liu, H. *Heat Exchangers*, 2nd ed.; CRC Press: Boca Raton, FL, 2002; p 520.
(61) Bondy, F.; Lippa, S. Heat Transfer in Agitated Vessels. *Chem. Eng.* **1983**, *90*, 62−71.
(62) Sukhatme, S. P. *Textbook of Heat Transfer*, 4th ed.; Universities Press: Hyderabad, India, 2005.
(63) Ekpo, E.; Mujtaba, I. Evaluation of Neural Networks-Based Controllers in Batch Polymerisation of Methyl Methacrylate. *Neurocomputing* **2008**, *71*, 1401−1412.
(64) Daoutidis, P.; Soroush, M.; Kravaris, C. Feedforward/Feedback Control of Multivariable Nonlinear Processes. *AIChE J.* **1990**, *36*, 1471−1484.